



Contents lists available at ScienceDirect

## Journal of Materials Research and Technology

journal homepage: [www.elsevier.com/locate/jmrt](http://www.elsevier.com/locate/jmrt)

## Frictional stability of pumice-reinforced lightweight magnesium composite in ambient and elevated temperature environments

Venkatesh Chenrayan<sup>a,\*\*</sup>, Kiran Shahapurkar<sup>b,\*\*\*</sup>, Chandru Manivannan<sup>c</sup>,  
Manzoore Elahi M. Soudagar<sup>d,e,f</sup>, Yasser Fouad<sup>g</sup>, M.A. Kalam<sup>h</sup>, Muhammad Mahmood Ali<sup>i,j,\*</sup>,  
Muhammad Nasir Bashir<sup>k,l,\*\*\*\*</sup>

<sup>a</sup> AU-Sophisticated Testing and Instrumentation Centre (AU-STIC), Department of Mechanical Engineering, Alliance School of Applied Engineering, Alliance University, Bengaluru, 562106, India

<sup>b</sup> Centre of Molecular Medicine and Diagnostics (COMMAND), Saveetha Dental College and Hospitals, Saveetha Institute of Medical and Technical Sciences, Saveetha University, Chennai 600 077, India

<sup>c</sup> Department of Mechanical Engineering, Dhirajlal Gandhi College of Technology, Salem, India

<sup>d</sup> Department of Mechanical Engineering, Graphic Era (Deemed to be University), Dehradun, Uttarakhand, 248002, India

<sup>e</sup> Centre of Research Impact and Outcome, Chitkara University, Rajpura, 140417, Punjab, India

<sup>f</sup> Division of Research and Development, Lovely Professional University, Phagwara, Punjab, India

<sup>g</sup> Department of Applied Mechanical Engineering, College of Applied Engineering, Muzahimiyah Branch, King Saud University, P.O. Box 800, Riyadh, 11421, Saudi Arabia

<sup>h</sup> School of Civil and Environmental Engineering, FEIT, University of Technology, Sydney, NSW, 2007, Australia

<sup>i</sup> Centre for Mathematical Modelling and Intelligent Systems for Health and Environment (MISHE), Atlantic Technological University Sligo, Ash Lane, F91 YW50, Sligo, Ireland

<sup>j</sup> Department of Mechatronic Engineering, Atlantic Technological University Sligo, Ash Lane, F91 YW50, Sligo, Ireland

<sup>k</sup> Department of Mechanical Engineering, College of Electrical and Mechanical Engineering, National University of Sciences and Technology, Islamabad, 46060, Pakistan

<sup>l</sup> Department of Mechanical Engineering, Yonsei University, Seoul, 120-749, Republic of Korea

## ARTICLE INFO

Handling editor: SN Monteiro

## Keywords:

Pumice  
Squeeze casting  
Adhesive wear  
Abrasive wear  
Oxide layers  
Coefficient of friction

## ABSTRACT

Lightweight materials with better resistance to sliding wear are prominent candidates for automobile brake drums, clutch pads and cylinder block applications to facilitate fuel economy. This attempt is reserved to cater to materials with higher tribological quality needs. Less dense foamy pumice stone particles were involved in three different percentages (5, 10, and 15 wt%) to reinforce lightweight AZ31 Mg alloy. A stir-assisted squeeze casting technique was pursued to process the composite and refine the grain structure. A phase detection, elemental mapping and microstructure study were done through X-ray diffraction (XRD), energy dispersive spectroscopy (EDS), and scanning electron microscopy (SEM), respectively. An experimental dry sliding wear scrutiny was administered using a pin-on-disc apparatus by considering: (i) ambient and elevated temperature environments and (ii) three different levels of loads. The results reveal a significant drop in wear loss and a frictional coefficient for 15% pumice-loaded composite than the base alloy. Post-wear examination acknowledges the fact that the ambient temperature wear is governed by adhesive-abrasive wear and high temperature is by abrasive wear mechanisms. Worn-out scrutiny authenticates the presence of oxide layers and their role in lubrication. A comparative study with previous works upholds the novel magnesium composite is the right candidate for the mentioned automobile applications.

\* Corresponding author. Centre for Mathematical Modelling and Intelligent Systems for Health and Environment (MISHE), Atlantic Technological University Sligo, Ash Lane, F91 YW50, Sligo, Ireland.

\*\* Corresponding author. AU-Sophisticated Testing and Instrumentation Centre (AU-STIC), Department of Mechanical Engineering, Alliance School of Applied Engineering, Alliance University, Bengaluru, 562106, India.

\*\*\* Corresponding author. Centre of Molecular Medicine and Diagnostics (COMMAND), Saveetha Dental College and Hospitals, Saveetha Institute of Medical and Technical Sciences, Saveetha University, Chennai, India.

\*\*\*\* Corresponding author. Department of Mechanical Engineering, Yonsei University, Seoul, 120-749, Republic of Korea.

E-mail addresses: [venkyachvsh@yahoo.co.in](mailto:venkyachvsh@yahoo.co.in) (V. Chenrayan), [kiranhs1588@gmail.com](mailto:kiranhs1588@gmail.com) (K. Shahapurkar), [mechchandru123@gmail.com](mailto:mechchandru123@gmail.com) (C. Manivannan), [me.soudagar@gmail.com](mailto:me.soudagar@gmail.com) (M.E.M. Soudagar), [yfouad@ksu.edu.sa](mailto:yfouad@ksu.edu.sa) (Y. Fouad), [mdabul.kalam@uts.edu.au](mailto:mdabul.kalam@uts.edu.au) (M.A. Kalam), [Muhammad.Ali@atu.ie](mailto:Muhammad.Ali@atu.ie) (M.M. Ali), [nasir@yonsei.ac.kr](mailto:nasir@yonsei.ac.kr) (M.N. Bashir).

<https://doi.org/10.1016/j.jmrt.2024.08.153>

Received 5 January 2024; Received in revised form 19 August 2024; Accepted 22 August 2024

Available online 24 August 2024

2238-7854/© 2024 The Authors. Published by Elsevier B.V. This is an open access article under the CC BY license (<http://creativecommons.org/licenses/by/4.0/>).

## 1. Introduction

Fuel consumption of automotive vehicles is a bigger challenge for any automobile manufacturer to survive in the global competition. The advanced engine technology and weight reduction of key auto parts are the predominant ways to sustain in the market for any manufacturer [1]. Since fuel consumption is inversely proportional to the weight of the vehicle, the manufacturers are keen on developing automobile components from low specific weight material without compromising its specific strength aspect [2–4]. The Al composite is the one, which caters for this need of the industries. However, continuous improvement is a core agenda in any industrial management policy, which leads to the development of components from the Mg composite owing to its 35% lesser density than Al by compromising its higher cost than Al [5]. Further involvement of porous syntactic [6] and ceramic foams [7] as a potential reinforcement to process a wider variety of less-dense Mg composite has already been attempted. A pumice is a known low-dense ceramic foam capable of floating in water, largely available in Ethiopia [8]. A pumice, a by-product of volcanic eruption is available in the density range of 0.24–0.48 g/cm<sup>3</sup> according to the subset, where it exists [9]. Yellowish pumice stones are abundantly available in Awash National Park, Ethiopia. It is a tactical approach to include pumice ceramic foam to develop newer varieties of Mg matrix composite to address automobile applications specifically, anticipating wear resistance. Apart from the reinforcement, the processing route also has an influencing role in deciding the properties of the composites. There are a variety of both liquid and solid routes of processing techniques to render the metal matrix composites [10]. However, squeeze-assisted stir casting was reported to be versatile in developing a composite with good microstructure refinement and a void-free nature [11].

Gupta et al. [12] conducted an extensive literature survey on syntactic foam-reinforced magnesium composite. The different sizes of cenosphere and their influence on reduction in density and improvement in mechanical properties were deeply discussed. The report highlighted that the ceramic content available in the cenosphere is the prime agent in escalating the properties. Xie et al. [13] prepared a Mg composite reinforced with SiC and administered a dry sliding wear study to estimate the wear characteristics of the composite. The test results revealed that the higher increment in SiC minimizes the wear loss. At a higher level of normal load, the brittle failure of the tribo-layer is reported. Banerjee et al. [14] developed a Mg composite loaded with varying weight proportions of WC nanoparticles through stir-casting techniques. A substantial improvement in microstructure and wear behaviour was reported in comparison with the base material. Turan et al. [15] carried out a tribological study on a hybrid Mg composite reinforced with multi-walled carbon nanotubes (MWCNTs) and graphene. The nanofillers influenced the microstructure and inflated the hardness and wear resistance. Shen et al. [16] examined the wear behaviour of nano-SiC-reinforced Mg composite against different sliding velocities and normal loads. The strengthening mechanism achieved through the inclusion of nano-SiC particles offered a wear resistance in multiple folds in comparison to the base alloy. The worn-out analysis revealed the transformation of wear damage from delamination to plastic deformation, as the normal load increases.

Dinaharan et al. [6] synthesized Mg matrix composite reinforced with a 10 wt% of fly ash in two different processing routes: stir casting and friction stir processing and evaluated the tribological behaviour against a dry sliding wear test. The authors claimed that an 18 % reduction in density was achieved for a 10 wt% of fly ash reinforced composite when compared to the neat Mg. According to this study, the processing approach had a greater influence on the wear behaviour of the composite because the stir-casting process produced a microstructure with vivid inhomogeneity and coarse grain structures. In contrast, friction stir processing delivered a microstructure with homogenous dispersion of fly ash particles and better grain refinement. The sliding wear test showed a higher weight loss to the material processed through

stir casting than the friction stir processing. Manakari et al. [17] attempted a synthesis of Mg metal matrix composite reinforced with two different wt.% of micro balloons: 15, 25 through Disintegrated Melt Deposition (DMD) and examined density, hardness, and wear loss. The report declared that a 17 % and 250 % reduction in density and wear damage was attained respectively when compared to the base alloy. The ceramic contents present in the reinforcement and the protective tribo-layer formed due to the oxide formation retarded the material loss. Yu and Huang [18] documented their findings on the examination of the wear phenomenon on AZ91 Mg alloy reinforced with fly ash particles with five different diameters varying from 40 to 150 µm. The authors reported that the wear loss was predominantly more for pure AZ91 alloy than the composite. The effect of the diameter of the fly ash particles was found to be more influential in dictating the wear since the higher-diameter particles exposed the reinforcement much more than the matrix material.

In this study, abundantly available mineral waste, a pumice stone particle is pressed into reinforcement to cast AZ31 Mg alloy composite through stir stir-assisted squeeze casting technique. Furthermore, the performance of Mg composites in terms of density, hardness, and wear properties has been investigated. The ultimate object of the proposed study is to figure out a very lightweight material with an excellent wear resistance ability, to recommend the same for automobile brake drums and clutch plate applications. Already, many research attempts have been successfully made to identify lightweight Mg composite reinforced with a variety of porous particles like syntactic foam, glass micro balloons, cenospheres etc. However, none of the research attempts has been recorded to reinforce foamy rock pumice particles so far. Further, the experimental investigation of wear characteristics of developed Mg composite both at room temperature and elevated temperature is considered to be a unique attempt and also a crown of novelty. Rigorous wear experimentation by varying the wt.% of pumice particles, further worn-out surface analysis and density analysis are conducted to promote the material as the right candidate for automobile brake drums and clutch plate applications.

## 2. Materials and methods

### 2.1. Materials

Metal Mart in Coimbatore, India delivered a 2 kg AZ31 Mg alloy rod. Fig. 1 shows pumice stones gathered from Awash National Park, near Adama state capital, Ethiopia. To unleash insects and worms, the gathered stones were heated to 150° C in an open environment. The preheated pumice stones were reduced to 30 µm, and the size was controlled using a 30 µm sieve as authenticated by the particle analyzer results shown in Fig. 1(b). The mechanical properties of AZ31 Mg alloy and pumice porous stone are shown in Table 1. The chemical composition of AZ31 Mg alloy and pumice are shown in Tables 2 and 3, respectively.

### 2.2. Processing of Mg-pumice composite

A stirrer-assisted squeeze casting unit was employed for the processing and the casting parameters are listed in Table 4. The moisture and surface contaminants present in the pumice powder were removed by pre-heating the pumice powder to 250°C in an open crucible kept inside an electric furnace. Then, 0.5 kg of AZ31 Mg alloy was melted in the same manner until it reached 850° C, transforming it into a molten liquid bath. To reduce the severe combustion of AZ31, a mixture of CO<sub>2</sub> and SF<sub>6</sub> was injected into the furnace at a temperature of 250 °C, subsequently, an Argon gas was fed into the furnace at 600 °C to eliminate the oxidation process [20]. The molten bath was kept at 800 °C for 15 min and then, the prepared pumice particles were added to the molten bath. A graphite-coated stirrer made up of stainless steel, whose blades were arranged at an angle of 30° to the axis of the stirrer, was utilized to

stir the molten bath. A stirrer fitted with an electric motor was made to rotate at 600 rpm for 10 min, to disperse the pumice particles uniformly throughout the molten bath. The wettability between pumice particles and Mg matrix was maintained with the addition of 1 g of Al to the molten bath [21]. The molten bath was fed into the squeeze casting unit whose die (30 mm diameter × 250 mm length) and plunger were pre-heated to 300 °C to prevent air quenching. The plunger was made to compress the molten bath at 120 MPa pressure and the action of compression was preserved until 60 s to exhaust the porosities. The entire process was repeated until the casting of three different composite rods with varying pumice particle of 5, 10, and 15 wt% [22]. The test specimen pins were machined to the standard dimensions of 10 mm diameter and 20 mm length. P5, P10, and P15 are the notations used throughout the article to represent 5, 10, and 15 wt% of pumice particle inclusion respectively.

### 2.3. Characterization

The phase composition and microstructure of the composite specimens were examined through XRD and SEM, respectively. Energy dispersive spectroscopy was pressed into the service for elemental study of pumice particles. As a part of specimen preparation for SEM investigation, 10 mm side cubes were machined through Wire-cut EDM and their surfaces were buffed with an emery sheet. A Zeiss PV-FE SEM and XRD test (Malvern Panalytical, UK) were used for the microstructure and phase analyses respectively. The real density of the composite material was determined using a density measuring instrument (Mettler Toledo, USA) working under Archimedes' displacement principle. The theoretical density ( $\rho_d$ ) and the percentage of porosity ( $P$ ) of the composite material were predicted using the rule of mixture.

### 2.4. Wear and hardness tests

A DUCOM (Bangalore, India) pin and disc wear testing apparatus was utilized for the dry sliding wear test. The wear assessment was done by using a counterpart EN30 grade disc with an 80 HRC hardness and 0.15  $\mu\text{m}$  surface roughness. The sliding distance, disc rotation, and sliding velocity were all kept constant at 1.5 km, 600 rpm, and 3 m/s, respectively. A high-temperature wear test was performed on a secondary disc. Three different levels of normal loads: 25, 50, and 75 N were chosen for both room and elevated temperature wear tests. A room temperature test was conducted at 28 °C, whereas an elevated temperature test was at 250 °C. To obtain statistically meaningful results: at each load and temperature, three specimens were evaluated and their average value was considered for further analysis. The three levels of load changing were done by using a pneumatically operated and computer-controlled load-changing system. Every elevated temperature test was started after ensuring that the disc had reached the stipulated

**Table 1**

Physical and mechanical properties of AZ31 Mg alloy and pumice stone [6,19].

Material	Melting point (°C)	Density (gm/cm <sup>3</sup> )	Tensile strength (MPa)<	Hardness (BHN)
Magnesium AZ31	630	1.77 ± 0.035	260 ± 12	51HV
Pumice	3652	0.28 ± 0.015	78 ± 3.45	6 HM

temperature. Before the experiment began, the disc was polished every time using a 120-grade commercial emery followed by acetone rinsing. The frictional force and pin height loss were assessed using a fully computerized data-collecting system. The volume loss of material was used to compute the wear rate with the help of the following relation [11],

$$W_r = \frac{v_s - v_e}{sd_s - sd_e} \quad (1)$$

where

$v_s$  The volume of the pin before the start of the test

$v_e$  The volume of the pin after the test

$sd_s$  Sliding distance before the start of the test

$sd_e$  Sliding distance after the test

Then, the wear rate and coefficient of friction can be computed with the following equations (2) and (3), respectively [11].

$$W_s = \frac{W_r}{F} \quad (2)$$

$$\mu = \frac{F}{F_n} \quad (3)$$

where  $F_n$  and  $F$  are normal and frictional forces, respectively.

The hardness was estimated as per ASTM E 92 standard (25 mm × 25 mm × 10 mm specimens) using a micro-hardness tester (Vickers scale-ZwickRoell Corporation) with a testing load capacity of 1 kg.

## 3. Results and discussion

### 3.1. Density evaluation

The theoretical density computed from the rule of mixture equation and the density measured experimentally has been furnished in Table 5. The ratio between the density difference between theoretical and experimental to the theoretical density is considered to be a void fraction. The results declare the maximum void percentage is 0.252 which indicates the fabricated composites are in near porous free structure.

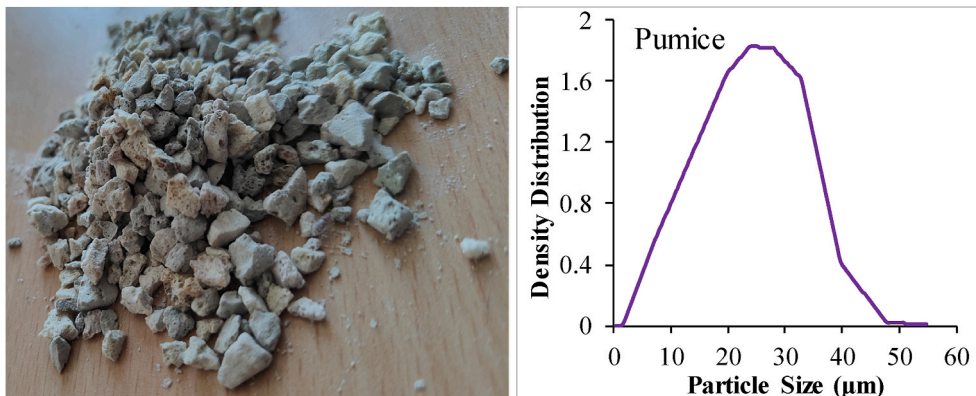


**Fig. 1.** Reinforcements and their size (a) a heap of pumice stones (b) size analyzer result.

The squeeze casting process and its holding time collectively help the composite to reach negligible porosity. The introduction of lightweight pumice particles prompts the composite to lose its density, in comparison with the base alloy. The weight saving to the scale of 12.8 % is achieved from the higher level of inclusion of pumice particles (P15) when compared to the base alloy.

### 3.2. Characterization of novel Mg composite

The microstructure of the novel Mg composite, the reinforcement dispersion and the grain refinement are depicted in Fig. 2(a)–(d). The SEM micrograph shown in Fig. 2 (a) affirms the existence of pumice particles which are dispersed uniformly. The intricate structure of pumice particles with exclusive porous regions divided by the wall structure and tubular vesicle structure [8] is well authenticated through Fig. 2 (b). It can be seen from micrographs from Fig. 2(a)–(c), that some of the micropores of pumice particles have been stuffed with matrix material and a few of the particles are left unfilled. The unfilled pumice particles are the root cause of the density loss of the composite. The heterogeneous nucleation of eutectic phases MgO and Mg<sub>2</sub>Si developed at the interfaces of pumice particles and the matrix materials are thoroughly identified in Fig. 2 (c). A 120 MPa of pressure utilization, its holding time and the inclusion of foreign particles lower the energy barrier and subsequently reduce the activation energy required to form many eutectic phases. Thus, the pressure building helps the nucleated eutectic phases around the pumice particles to grow in a dendrite structure, which is acknowledged by Fig. 2 (c). The pressure exerted by the squeeze casting technique eliminates the possible porosity induced at the time of solidification. An expeditious movement of dislocation caused by the compression forms a thicker grain boundary and in turn, paves the way for better grain refinement as shown in Fig. 2 (d). A similar observation was recorded by the researchers [6] and reported in their document which dealt with magnesium composite reinforced with fly ash particles. The authors explored the possible eutectic phases MgO and Mg<sub>2</sub>Si developed along with ceramic compounds Al<sub>2</sub>O<sub>3</sub> and SiO<sub>2</sub> available from fly ash.

Fig. 3 shows the elemental analysis for pumice particles observed through EDS. The results manifest the prominent peaks showing Si, O and C and smaller peaks corresponding to Al and Fe. The elemental composition of pumice particles shown in Table 6 confirms the elements that are possible to form potential ceramic compounds SiO<sub>2</sub> and Al<sub>2</sub>O<sub>3</sub>, to the contribution of more than 88 %. This data authenticates the pumice is the right candidate for inclusion as reinforcements (see Table 7).

Fig. 4 depicts the elemental analysis conducted for the P15 specimen through EDS. Larger peaks reflect the magnesium, but significant peaks are observed for Al, Si, C and O where their overall contributions can be observed around 30 %. The results explored the availability of promising elements to form significant ceramic compounds in a considerable quantity.

The XRD results conducted for the P15 specimen are illustrated in Fig. 5. The results endorse the presence of two different ceramic compounds: silica and alumina, and are detected in a significant peak at 27.2° and 33.99° on the 2θ position. The existence of intermetallic phases MgO and MgSi<sub>2</sub> identified in SEM micrographs (see Fig. 2) is validated through XRD results.

### 3.3. Hardness

The hardness test was conducted on three different variants of

**Table 2**  
Chemical constituents of AZ31 Mg alloy.

Magnesium	Aluminum	Zinc	Manganese	Silicon	Copper	Calcium
97	2.5–3.6	0.6–1.5	0.2	0.1	0.05	0.04

**Table 3**  
Chemical constituents of pumice [19].

SiO <sub>2</sub>	Al <sub>2</sub> O <sub>3</sub>	Fe <sub>2</sub> O <sub>3</sub>	CaO	Ni <sub>2</sub> O	K <sub>2</sub> O
74.43%	12.83%	1.83%	1.56%	4.37%	4.37%

**Table 4**  
Stir cum squeeze casting variables [23].

Variable names	Value
Conditioning temperature of reinforcements (°C)	250
Stirring temperature (°C)	850
Stirring duration (min)	10
Stirrer rotation (rpm)	600
Squeezing pressure (MPa)	120
Preheated die temperature (°C)	300
Punch holding time under pressure (sec)	60

**Table 5**  
Theoretical and experimental densities of all variants of the composite.

Pumice weight fraction (%)	Theoretical density (gm/cm <sup>3</sup> )	Experimental density (gm/cm <sup>3</sup> )	Void fraction (%)
P5	1.6955	1.6935 ± 0.067 00.0. ±0.0575	0.11
P10	1.6210	1.6184 ± 0.056	0.156
P15	1.5460	1.5421 ± 0.064	0.252

pumice along with base alloy and their respective hardness values are shown in Fig. 6. It can be seen from the results that the proportionate increment in hardness is observed for every incremental step of pumice addition. P15 coupons register nearly 55.5 % of additional hardness than the base alloy. This phenomenal increment may be attributed to two factors: the addition of pumice particles, and grain refinement achieved through squeeze casting. The influence of pumice particles in inflating the hardness can be correlated to the ceramic contents in the pumice particles. The finer grain structure attained through pressurized compaction leads to a supplementary increment in hardness. The Hall-pitch [24] reciprocal relation between the hardness and grain size advocates that the lesser the grain size, the higher the hardness.

### 3.4. Room temperature wear analysis

The wear rate computed from the wear test conducted for three different variants of pumice composites along with base alloy at room temperature is shown in Fig. 7(a)–(c). The influence of increasing load and increasing sliding distance on the wear rate is observed in the results. A linear increment in wear rate is recorded for every incremental step of sliding distance, similarly, wear rate increased with increasing load irrespective of the filler content. However, a decreased wear rate is witnessed for the increasing content of pumice particles, even at ascending load. Fig. 7 (a), shows a mild wear rate at 25 N load because all curves reflect steady-state wear until 750 m of sliding distance, after which a significant spike in wear rate is observed. The interlocking of asperities at this juncture seems stronger against the lower magnitude of load, hence the asperities are subject to plastic deformation only. The continuous engagement of asperities with the counter body for a longer period (rest of the sliding distance 750 m–1500 m) under the load, prompts the weaker asperities to detach, causing more wear rate. The comparison of results manifests that at a higher load of 75 N shown in

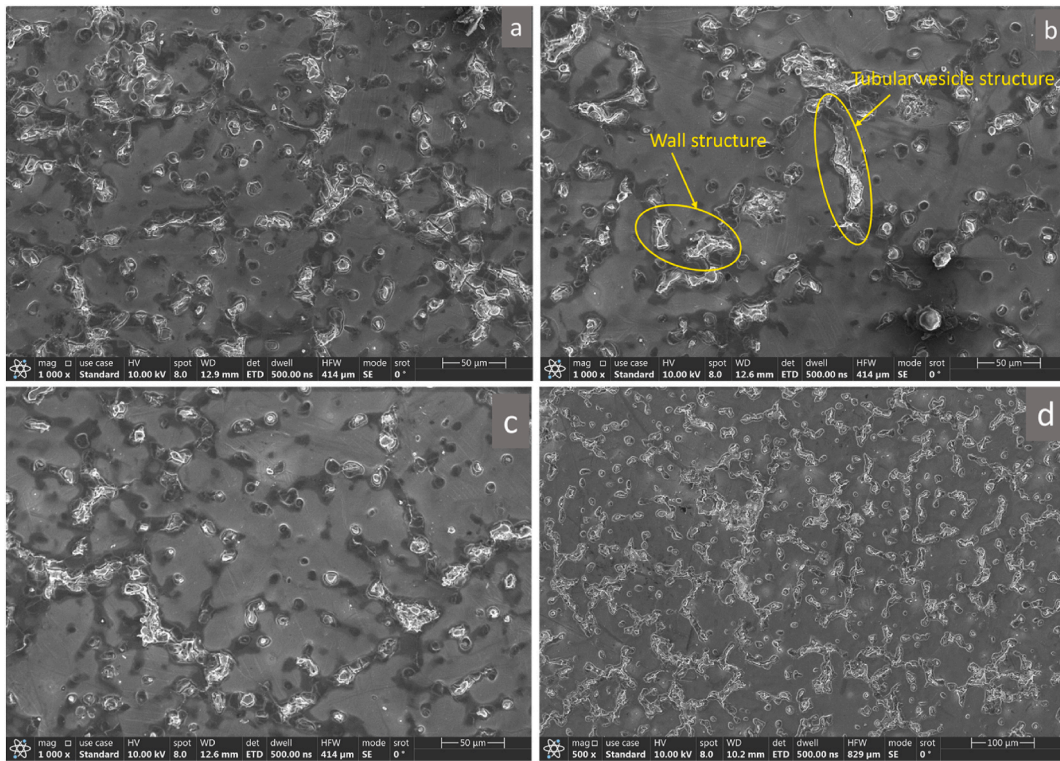


Fig. 2. SEM micrographs of P10 (a) Homogenous dispersion of pumice particles (b) Porous structure of pumice (c) Dendrite eutectic phase (d) Finer grain structure.

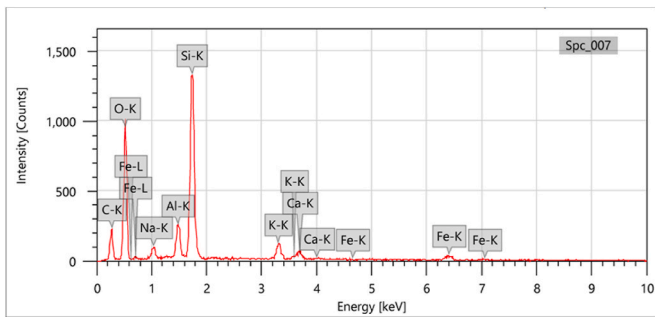


Fig. 3. EDS spectrum of pumice particles.

Table 6  
Elemental composition of pumice particle.

Elements	Mass (%)	Atom (%)
C	22.07	31.09
O	50.31	53.20
Na	1.78	1.31
Al	3.21	2.01
Si	16.99	10.24
K	2.37	1.02
Ca	1.23	0.52
Fe	2.04	0.62

Fig. 7 (c), the base alloy exhibits 210 % more wear loss than the P15 specimen. The wear resistance behaviour of pumice-reinforced specimens is developed due to the inherent ceramic nature of the silica and alumina available in pumice particles. Additional wear resistance is offered by the formation of oxide layers which act as a lubricant layer to protect the sub-surfaces by mating with each other. It is interesting to view the steady state nature of P15 even at higher loads 50 N shown in Fig. 7 (b) and at 75 N until 1/3rd of the sliding distance. The steady state

Table 7  
Elemental compositions of P5 composite.

Elements	Mass (%)	Atom (%)
C K	11.41	19.55
Fe K	7.86	17.83
Na K	3.06	2.74
Mg K	63.55	53.81
Al K	6.99	3.04
Si K	7.13	3.02

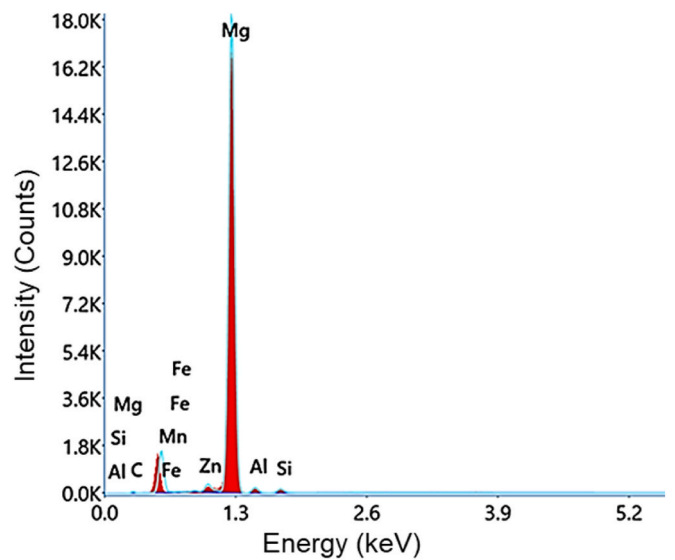


Fig. 4. EDS Spectrum of P5 composite.

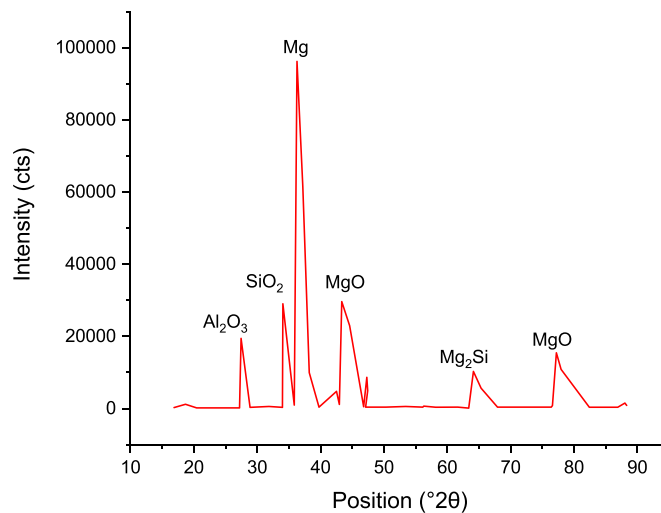


Fig. 5. XRD spectrum of P15 specimen.

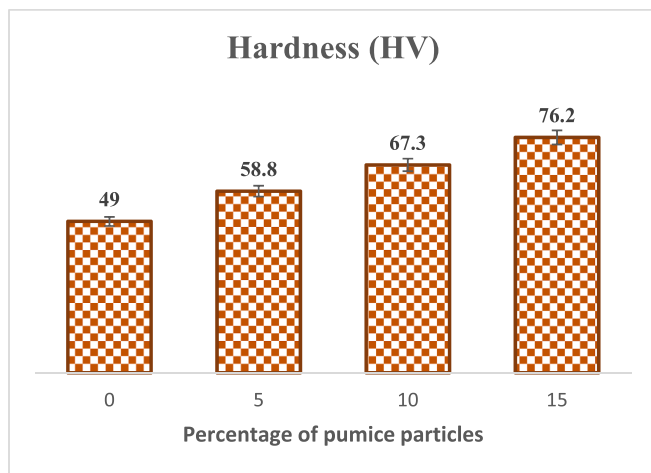


Fig. 6. Hardness results recorded for different pumice variants.

implies the two-body abrasion [20], where the material loss is minimal. On the other hand, a steep rise in material loss for all the variants during the second half of the sliding distance is considered to be a three-body abrasion [25], which intensifies the material loss. Already detached asperities between the surfaces of the specimen and counter body act as a third body to accelerate the wear mechanism [11,26]. A very similar trend of wear loss was reported by the researchers [27] while they experimented with a wear study of AZ91D Mg alloy reinforced with 3 wt % of silicon carbide and graphite. They revealed the same nature of increasing wear with increasing load and sliding velocity. The authors reported that 0.012 mm<sup>3</sup>/m of material loss for the higher inclusion of SiC and graphite at 60 N normal load and 2.618 m/s of sliding velocity. The declaration and findings are concurrent with this study. Fig. 7 (d) depicts a bar chart showing consolidated values of wear rate.

Fig. 8(a)–(c) depicts the coefficient of friction (CoF) results obtained from the ratio between the frictional force to the normal load and Fig. 8 (d) illustrates the consolidated values of CoF through a bar chart. The results explored that the average CoF is recorded for pumice particle reinforced specimens substantially lower than the average CoF of base alloy. Comparative analysis manifests a 2.62 times of improvement in CoF is achieved for the P15 coupons in comparison with the base alloy. The improvement of the tribology index is attributed to the reduced magnitude of frictional forces owing to the hard nature of asperities built from P15 which resists the deformation. However, the relation between

the frictional force and hardness is complex. The harder surface resists the plastic deformation of asperities, and subsequently lesser adhesion between the asperities. Consequently, lesser adhesion is a clear signature of lesser frictional forces. Further, the improvement in CoF is supplemented by the fine grain structure (see Fig. 2 (d)) resulting from squeeze casting. A concurrence observation was made by the researchers [28] when they synthesized AZ31 Mg alloy reinforced varying wt % of Al<sub>2</sub>O<sub>3</sub> and CNTs. The authors conducted a wear study on exhaustive variation of inclusions of Al<sub>2</sub>O<sub>3</sub> and CNTs (3% Al<sub>2</sub>O<sub>3</sub>, 3% CNTs, 2% Al<sub>2</sub>O<sub>3</sub> + 1% CNTs, 1% CNTs + 2% Al<sub>2</sub>O<sub>3</sub>, 1.5% Al<sub>2</sub>O<sub>3</sub> + 1.5% CNTs), and reported that 2% CNTs + 1% Al<sub>2</sub>O<sub>3</sub> hybrid composite performed far better than rest of the combination at higher load by the impressive friction coefficient of 2.2. Nevertheless, the present study declares CoF of 1.44 at 75 N load for the same matrix material reinforced with foamy rock pumice, which interprets 34.5 % of significant improvement in tribological property than the mentioned previous study. Fig. 8 (d) depicts a bar chart showing consolidated values of CoF.

### 3.5. High-temperature wear analysis

The wear behaviour of all the variants of pumice-reinforced composite along with the base alloy at an elevated temperature of 250 °C is illustrated in Fig. 9(a)–(c) and Fig. 9 (d) shows a bar chart exploring consolidated values of wear rate. It is well understood that the wear is dictated by the normal load as well as the temperature. A comparative study between room temperature and high-temperature wear has disclosed the fact that the transformation of wear is observed from adhesive to abrasion at room temperature [29], whereas high-temperature wear is governed by pure abrasion [30,31]. At room temperature, adhesive wear due to interlocking of asperities continues until the detachment of asperities. Then the detached asperities act as a third body causing an abrasion, hence the transformation from adhesive to abrasion wear. At high temperatures, the material becomes softer while the counterpart is harder, and then naturally material loss happens due to the abrasion. Scientifically, abrasive wear is more dominant than adhesive wear which leads to more loss of material [32]. This phenomenon is reflected in the wear results: At higher load and temperature, 1%, 18%, 27% and 38% more wear are recorded than at room temperature for the specimens P0, P5, P10, and P15 respectively. The higher level of temperature and load accelerates the abrasion despite the inclusion of particles. However, within the high temperature, the wear rate of P5, P10, and P15 at a higher load of 75 N is 31.78, 33.6, and 35.65 % of less wear than the base alloy P0. The increase in wear resistance caused by the proportionate incremental addition of pumice particles is attributable not only to ceramic strengthening and hardening but also to the formation of oxide layers because magnesium is prone to oxidation at low temperatures. Nevertheless, at higher loads, the protective oxide layers encounter a brittle failure thereby exposing both the subsurface and causing more wear [33]. This phenomenon endorses the incremental wear loss of material at every incremental step of normal load, even if pumice particle addition is incremental.

Similar to that of room temperature wear, for high-temperature wear, steady state wear is observed for P0, P5, P10 and P15 specimens at lower levels of load. A minimal probability of brittle failure of oxide layers at lower-level load and the elastic deformation of the asperities ensures the wear at a steady state [34]. On the other hand, the wear rate is linear at a high level of load owing to the brittle failure of the oxide layers and the plastic deformation of the asperities. Kumar et al. [35] executed a high-temperature wear study on Al–4Cu alloy reinforced with 5 and 10% of TiB<sub>2</sub> at five different temperatures room temperature, 100, 150, 200, 250 and 300 °C subject to the normal loads varying at 10 N incremental step from 30 N to 130 N. They explored the influence of load and temperature on the wear rate of the developed novel material. The wear rate observed was changing from mild to severe for all temperature cases, the increased load induced the shift of mild wear to severe region. The authors reported steady-state wear similar to that of the

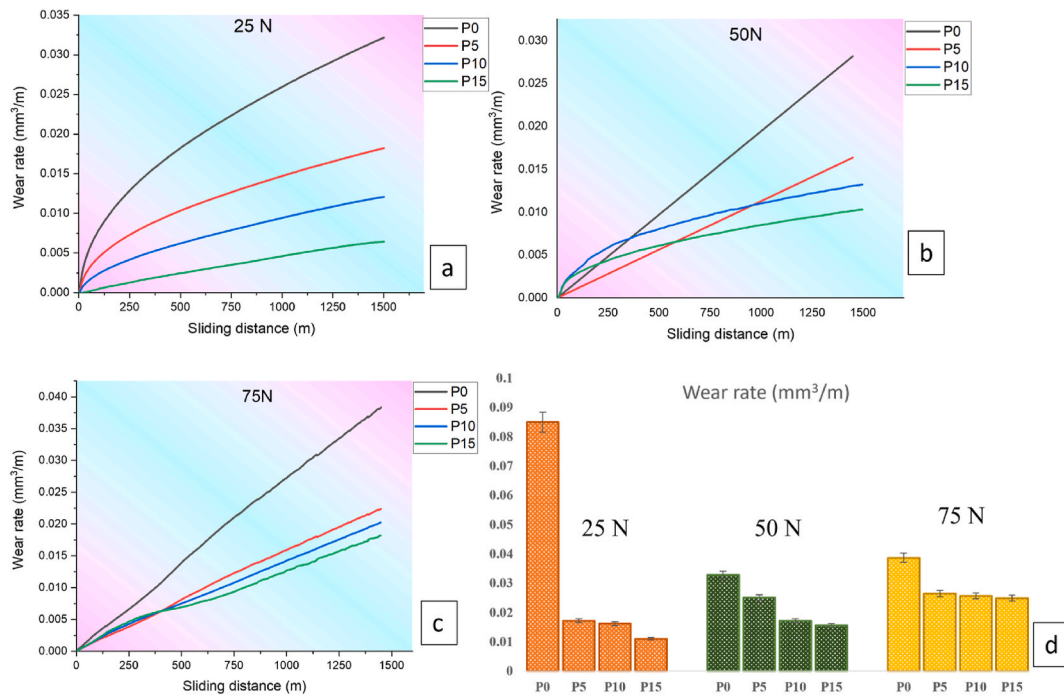


**Fig. 7.** Wear rate of all variants of pumice including base alloy at room temperature (a) At 25 N normal load (b) At 50 N normal load (c) At 75 N normal load (d) Consolidated bar chart.

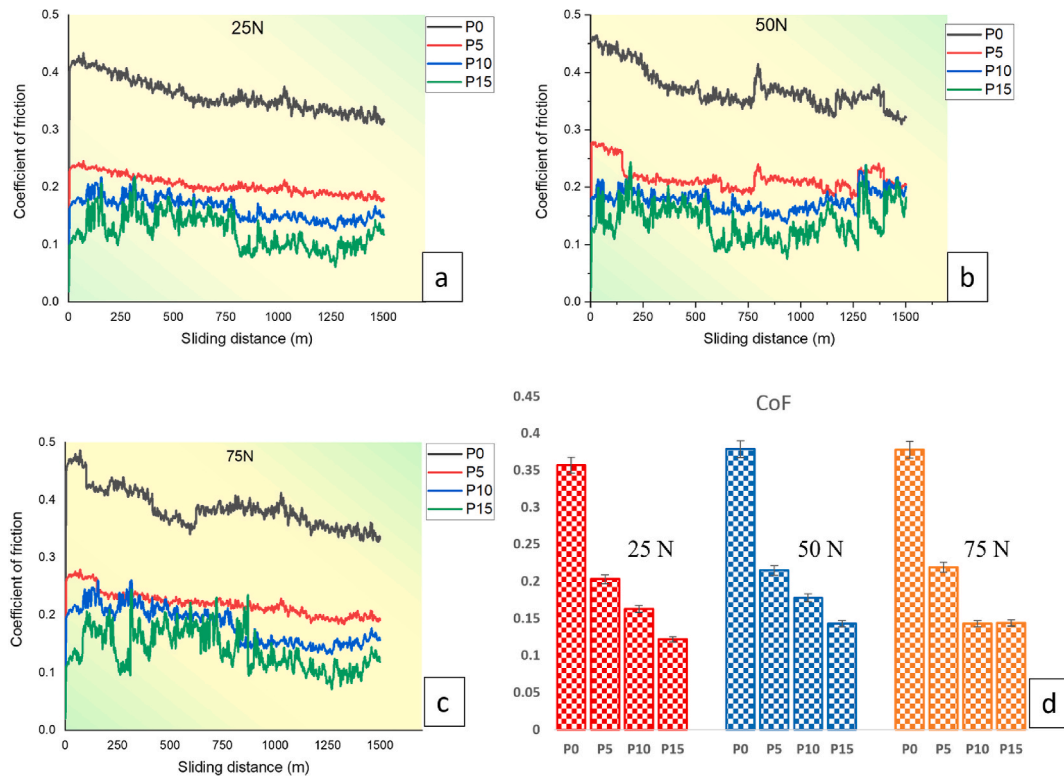


**Fig. 8.** Coefficient of friction calculated during room temperature study for all the variants of pumice (a) At 25 N (b) At 50 N (c) At 75 N (d) Consolidated bar chart.

present study, which advocated a steadiness in wear until 80 N for all cases of temperatures. The wear turned out to be severe beyond that region to the maximum load of 130 N. The minimum wear loss encountered at a steady state was claimed by the authors due to the improved hardness attained by the grain refinement, precipitation strengthening and dispersion strengthening. The severity of wear at

elevated load and temperature was viewed as three body abrasions between the ejected TiB<sub>2</sub> particles and thermally softened matrix material.

The results announce that the increased content of pumice particles records lesser wear even at high temperatures in comparison with base alloy P0. This improved performance is not only attributed to the increased tensile strength of the asperities supplemented by the ceramic

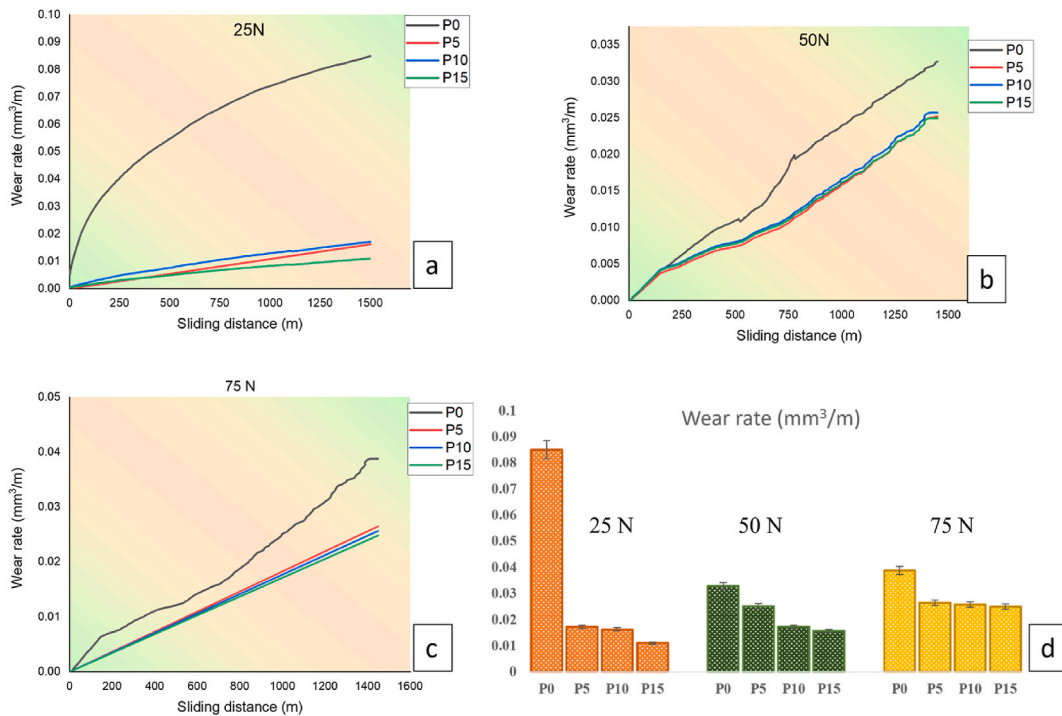


Fig. 9. Wear rate of all the variants of pumice composite including base alloy at 250 °C temperature (a) At 25 N (b) At 50 N (c) At 75 N (d) Consolidated bar chart.

content in the particles to resist the plastic deformation of the asperities but also to the oxide formation. The better grain structure availed through squeeze casting and increased hardness depicted in Fig. 6 also play a significant role in the descending wear rate at higher temperatures.

The distribution coefficient of friction for P0, P5, P10, and P15 at 25 N, 50 N, and 75 N normal loads during the high-temperature wear study is shown in Fig. 10(a)–(c), respectively and consolidated CoF values are

shown in Fig. 10 (d) as a bar chart. The descending trend of CoF is witnessed for the increasing content of pumice. The hard particles induce a substantial strength to the asperities to resist the plastic deformation, even at high temperatures, and then increased resistance minimizes the frictional force which reflects in the descending nature of CoF. As the wear rate becomes intensified with the increased load, the CoF is also an increasing trend with the load incremental. However, exceptional behaviour of CoF's descending trend concerning increased

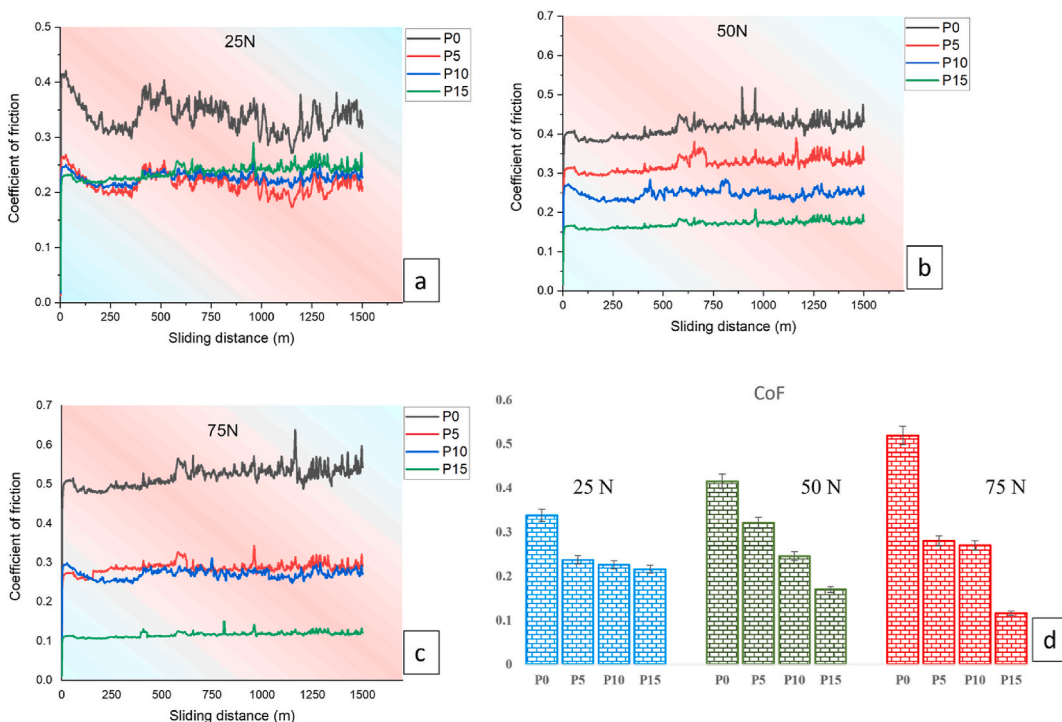


Fig. 10. Coefficient of friction calculated at 250 °C temperature for all the variants of pumice (a) At 25 N (b) At 50 N (c) At 75 N (d) Consolidated bar chart.



load is observed for P15. A significant reduction in CoF to the scale of 46.29 % is noticed for the P15 specimen at 75 N load than the same at 25 N load. This unique phenomenon reflects the behaviour of the material's constituents at high temperatures. The higher level of ceramic content available in P15, not only restricts the failure of asperities after the severe plastic deformation, but also brittle failure of the oxide layers formed. The absence of debris and fractured oxide layers, assures the lubricated nature of the surface, and subsequently minimum frictional force generated to curtail CoF. An identical finding was reported by the authors [36], while they attempted to investigate the high-temperature wear behaviour of Mg composite reinforced with boron nitride. The authors reported a minimal coefficient of friction of 0.25 at higher load and temperature of 20 N and 175 °C respectively for 0.25 % BN, claiming that the strengthening of matrix asperities with BN and Mg oxide layers were the prominent factors to minimize the frictional force.

### 3.6. Post-wear analysis

Evaluation of the wear rate and coefficient of friction and the related arguments can be backed up with surface textures obtained post-wear through SEM micrographs. As discussed earlier, room temperature wear is governed by adhesive-transformed abrasive wear. The worn-out surfaces and their textures, post room temperature wear test have been depicted in Fig. 11(a)–(d). The interlocking of asperities and their strength resist the surface adhesion, and hence the surface damage leaves with a wear mark. Further load intensifies causing abrading damage to the surfaces. Fig. 11 (a) and (c) are the comparative analysis of P5 and P15 specimens at 25 N respectively. For the same magnitude of load, P5 experiences a noticeable severe wear mark, whereas, P15 experiences a mild wear mark. However, both the nature of wear is in abrasion mode. The increased content of ceramic particles in P15 improves the hardness (see Fig. 6) and hence the resistance to indentation paves the way to mild wear. At a higher load (75 N), the surface examination is carried out for P5 and P15 through SEM observation and

the results are shown in Fig. 11(b)–(d) respectively. Wear rate results in sections 3.4 and 3.5 declare that the load is one of the catalysts to inflate the wear rate. It is authenticated in worn-out analysis through plough marks. Fig. 11 (b) shows the micrographs of P5 at 75 N, which explores dominant plough marks and detached asperities. The adhesive wear starts at 25 N and transforms into abrasive wear with the subsequent load increment to 75 N. The severe plastic deformation of the asperities at higher load, their detachment and their role as a third body to promote three-body abrasion are the road map of severe wear. The detached particles contribute to ploughing the surface significantly, which is captured in Fig. 11 (b). Instead, a mild indentation is recorded and is shown in Fig. 11 (d) for P15 at the same higher load. The negligible damage to the surface, even at peak load is attributable to the strengthening mechanism offered by the higher content of pumice particles and to the ability to resist severe plastic deformation.

As far as high-temperature wear is concerned, it is purely driven by the abrasion, since the material becomes softened at elevated temperature. Therefore, material loss due to wear is comparatively more than room temperature in all cases. The SEM micrographic results at high-temperature wear are shown in Fig. 12(a)–(d). The wear behaviour of P5 and P15 specimens at a lower-level load of 25 N is illustrated in Fig. 12 (a) and (c). A noticeable deeper erosion-like pit is witnessed in Fig. 12 (a) followed by complete brittle failure of the oxide layer formed. The broken oxide layers and their debris have been highlighted in Fig. 12 (a). However, minimum damage is evident for P15, without the oxide layer's failures shown in Fig. 12 (c). It is supplemented by elemental analysis and XRD results shown in Fig. 13 (a) and (b) that the formation of oxide layers is more pronounced for higher content of pumice particles. An excess oxygen present in the pumice particles contributes to the formation of dense oxide layers and results in decelerating the wear by acting as a lubricative layer to prevent metal-to-metal contact. The previous study [37] involving Mg matrix composite loaded with syntactic foam declared that the dispersion strengthening with syntactic foam and oxide formation is the prominent reason to

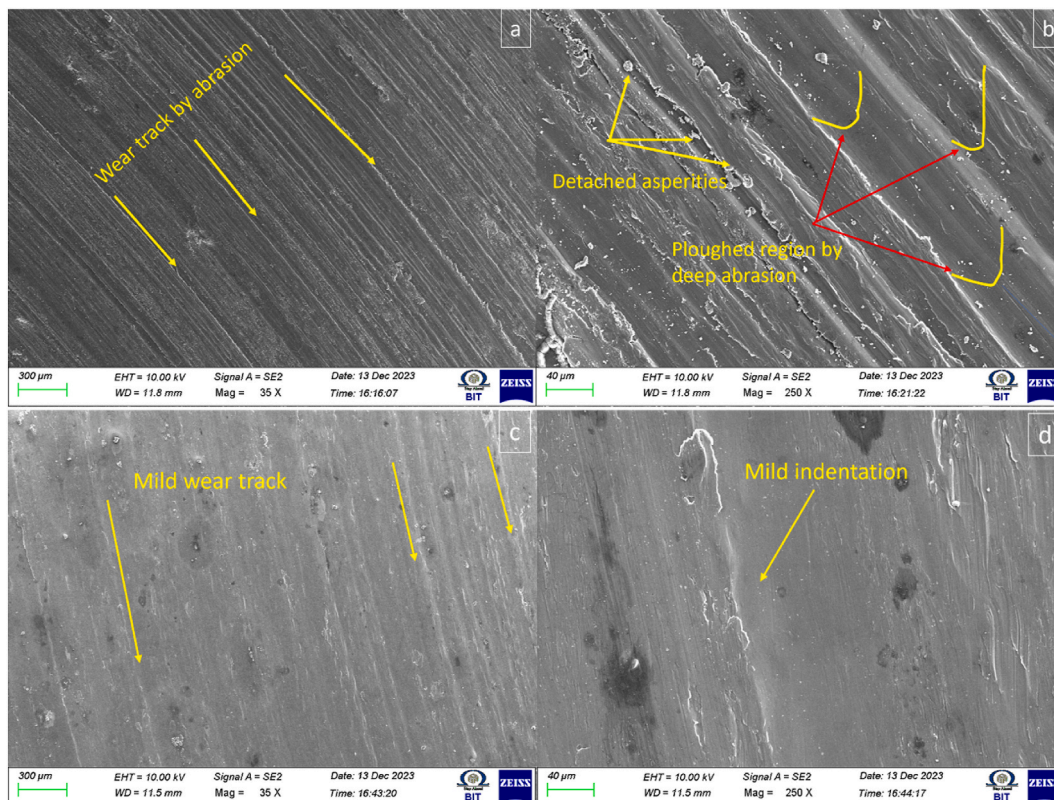


Fig. 11. Worn-out surface texture examination at room temperature (a) P5 on 25 N load (b) P5 on 75 N (c) P15 on 25 N load (d) P15 on 75 N load.

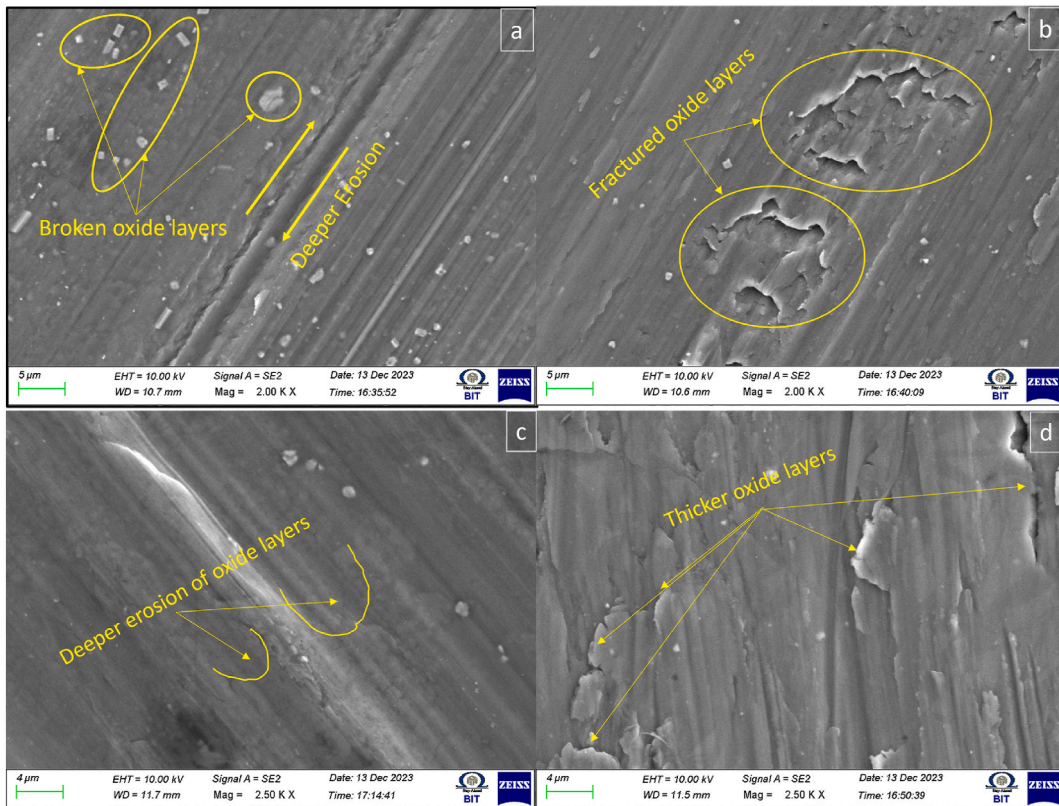


Fig. 12. Worn-out surface texture examination at 250 °C (a) P5 on 25 N load (b) P5 on 75 N (c) P15 on 25 N load (d) P15 on 75 N load.

retard the wear rate. The report highlighted the existence of magnesium oxide formation as a lubricative layer between sub-surfaces and its contribution to minimizing wear.

The comparison of wear characteristics of P5 and P15 at a higher level of load 75 N in an elevated temperature environment is shown in Fig. 12 (b) and (d). It is interpreted from Fig. 12 (b) that the higher load squeezes the oxide layer to fail and paves the way to metal-to-metal contact, thus more prominent wear is observed for P5 at 75 N load. Nevertheless, the higher content of pumice particles in P15 develops the oxide layers in a thicker manner, which safeguards the surfaces not to mat each other, and then minimum wear with deeper marks is seen. However, the impact of the 75 N load was also realized by witnessing the brittle failures of thicker oxide layers seen in Fig. 12 (d). It is quite obvious that the comparison of base alloy results is no longer beneficial to this discussion since it does not reflect the strengthening mechanism of particulate addition.

The worn-out surfaces are fed into XRD evaluation to study the possible oxide layer formation, and subsequently, the worn-out debris collected is also pressed into EDS analysis. Fig. 13 (a) and (b) depict the EDS and XRD results obtained for debris and worn-out surfaces respectively. EDS result affirms the presence of O<sub>2</sub> to react with the metal to form an oxide layer. The compound analysis conducted through XRD confirms the presence of MgO layers. The thicker oxide layer formation for P15 is acknowledged through a higher peak of MgO at 43.35° and 77.2° than the peaks available at the same 2θ position of P5.

#### 4. Conclusion

The investigation carried out to assess the tribological characteristics of newly developed novel lightweight Mg composite reinforced with foamy rock pumice corroborates the following illustrious conclusions.

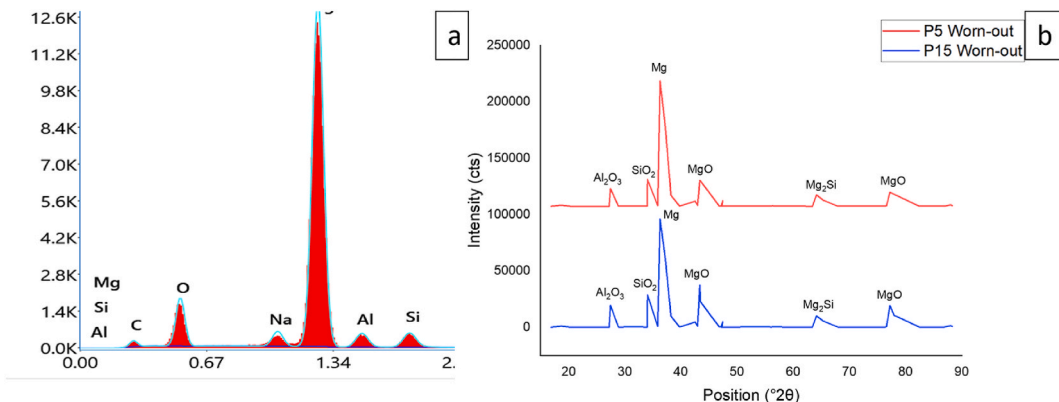


Fig. 13. (a) EDS result of debris (b) XRD result of worn-out surfaces.

1. The effect of squeeze casting and its holding time are found to be more influential in developing the fine grain structure which is revealed from microstructure study. Further, XRD analysis affirms the presence of ceramic compounds  $\text{Al}_2\text{O}_3$ ,  $\text{SiO}_2$  and intermetallic phases  $\text{MgO}$  and  $\text{Mg}_2\text{Si}$  in the novel Mg composite.
2. A 12.8 % weight saving and a lesser CoF value of 0.116 are observed for P15 than that of base alloy, which upholds the lightweight nature of the novel material to recommend the same for automobile brake drums and clutches applications.
3. The room temperature wear examination announces the wear is mitigated by adhesive wear and joining the hands with abrasive wear. However, it is found that the high-temperature wear is dictated by pure abrasion. The total wear loss recorded at room temperature for the base alloy is 210 % more than that of P15. However, P15 exhibits 38% higher wear loss at high temperatures than at room temperature.
4. A prominent drop in CoF is realized concerning the ascending addition of pumice particles both at room and elevated temperature circumstances. Post-wear analysis affirms a distinct nature of adhesive and abrasive wear through wear mark and plough mark respectively, subsequently, oxide formation and its brittle fractures are evident in post-wear analysis.

#### Declaration of competing interest

The authors declare that they have no known competing financial interests or personal relationships that could have appeared to influence the work reported in this paper.

#### Acknowledgements

The authors extend their appreciation to the Researchers Supporting Project number (RSPD2025R698), King Saud University, Riyadh, Saudi Arabia for funding this research work. Also, it is partly supported by YFL 2024, Yonsei University, Seoul, Republic of Korea.

#### References

- [1] Gupta N, Luong DD, Cho K. Magnesium matrix composite foams—density, mechanical properties, and applications. *Metals* 2012;2(3):238–52.
- [2] Rohatgi P, Weiss D, Gupta N. Applications of fly ash in synthesizing low-cost MMCs for automotive and other applications. *Jom* 2006;58:71–6.
- [3] Srivivas PD, Charoo M. Application of hybrid aluminum matrix composite in automotive industry. *Mater Today Proc* 2019;18:3189–200.
- [4] Heydarian A, et al. Effect of electrochemical parameters on wear and tribocorrosion capabilities of the PEO coatings generated through pulsed waveforms on AZ91 magnesium alloy. *J Mater Res Technol* 2023;27:6148–58.
- [5] Mordike B, Ebert T. Magnesium: properties—applications—potential. *Mater Sci Eng, A* 2001;302(1):37–45.
- [6] Dinaharan I, et al. Influence of processing route on microstructure and wear resistance of fly ash reinforced AZ31 magnesium matrix composites. *J Magnesium Alloys* 2019;7(1):155–65.
- [7] Chen J, Liu P, Song S. Preparation and compression performance of porous magnesium alloy composite with ceramic hollow spheres. *J Alloys Compd* 2022; 894:162397.
- [8] Çoban O, Yilmaz T. Volcanic particle materials in polymer composites: a review. *J Mater Sci* 2022;57(36):16989–7020.
- [9] Avcu E, et al. Possible use of volcanic ash as a filler in polyphenylene sulfide composites: thermal, mechanical, and erosive wear properties. *Polym Compos* 2014;35(9):1826–33.
- [10] Yu H. Processing routes for aluminum based nano-composites. MA: Worcester Polytechnic Institute Worcester; 2010.
- [11] Chenrayan V, et al. Tribological performance of TiB<sub>2</sub>-graphene Al 7075 hybrid composite processed through squeeze casting: at room and high temperature. *Tribol Int* 2023;185:108486.
- [12] Gupta M, Lai M, Saravananathan D. Synthesis, microstructure and properties characterization of disintegrated melt deposited Mg/SiC composites. *J Mater Sci* 2000;35:2155–65.
- [13] Xie Z, et al. Understanding the anti-wear mechanism of SiCp/WE43 magnesium matrix composite. *Vacuum* 2020;172:109049.
- [14] Banerjee S, et al. Dry sliding tribological behavior of AZ31-WC nano-composites. *J Magnesium Alloys* 2019;7(2):315–27.
- [15] Turan ME, Zengin H, Sun Y. Dry sliding wear behavior of (MWCNT+ GNP)s reinforced AZ91 magnesium matrix hybrid composites. *Met Mater Int* 2020;26: 541–50.
- [16] Shen M, et al. Dry sliding wear behaviour of AZ31 magnesium alloy strengthened by nanoscale SiCp. *J Mater Res Technol* 2022;16:814–23.
- [17] Manakari V, et al. Evaluation of wear resistance of magnesium/glass microballoon syntactic foams for engineering/biomedical applications. *Ceram Int* 2019;45(7): 9302–5.
- [18] Yu S, Huang Z. Dry sliding wear behavior of fly ash cenosphere/AZ91D Mg alloy composites. *J Mater Eng Perform* 2014;23:3480–8.
- [19] Kösedag E. Investigation of the effect of filling ratio on mechanical properties of pumice filled epoxy-based composites. *Gazi University Journal of Science Part C: Design and Technology*; 2023. 1-1.
- [20] Aathisugan I, Rose AR, Jebadurai DS. Mechanical and wear behaviour of AZ91D magnesium matrix hybrid composite reinforced with boron carbide and graphite. *J Magnesium Alloys* 2017;5(1):20–5.
- [21] Ye HZ, Liu XY. Review of recent studies in magnesium matrix composites. *J Mater Sci* 2004;39:6153–71.
- [22] Rohatgi P, et al. Microstructure and mechanical behavior of die casting AZ91D-Fly ash cenosphere composites. *Compos Appl Sci Manuf* 2009;40(6–7):883–96.
- [23] Mathimurugan N, et al. Room and high temperature tensile responses of TiB<sub>2</sub>-graphene Al 7075 hybrid composite processed through squeeze casting. *Nanomaterials* 2022;12(18):3124.
- [24] Cordero ZC, Knight BE, Schuh CA. Six decades of the Hall–Petch effect—a survey of grain-size strengthening studies on pure metals. *Int Mater Rev* 2016;61(8): 495–512.
- [25] Lim C, Lim S, Gupta M. Wear behaviour of SiCp-reinforced magnesium matrix composites. *Wear* 2003;255(1–6):629–37.
- [26] Zhao C, et al. Superior tribological and anti-corrosion performance of corrosion inhibitors intercalated LDH-MAO coating on AZ31 Mg alloys. *Tribol Int* 2024;191: 109126.
- [27] Girish B, et al. Wear behavior of magnesium alloy AZ91 hybrid composite materials. *Tribol Trans* 2015;58(3):481–9.
- [28] Lu D, Jiang Y, Zhou R. Wear performance of nano-Al<sub>2</sub>O<sub>3</sub> particles and CNTs reinforced magnesium matrix composites by friction stir processing. *Wear* 2013; 305(1–2):286–90.
- [29] Yong H, Li R. Effect of particulate reinforcement on wear behavior of magnesium matrix composites. *Trans Nonferrous Metals Soc China* 2012;22(11):2659–64.
- [30] Tan H, et al. Tribological performance and wear mechanisms of a high-temperature wear-resistant Al-Si/SiAlON composite. *Tribol Int* 2021;164:107227.
- [31] Wang W, et al. Effects of nanosecond laser shock peening on residual stress, corrosion and tribocorrosion behavior of WE43 magnesium alloys. *Wear* 2023; 524–525:204866.
- [32] Doddamani M. Wear behavior of glass microballoon based closed cell foam. *Mater Res Express* 2019;6(11):115314.
- [33] Ayyanar S, et al. Studies on high temperature wear and friction behaviour of AA6061/B 4 C/hBN hybrid composites. *Met Mater Int* 2021;27:3040–57.
- [34] Kumar NS, Suresh R, Shankar GS. High temperature wear behavior of Al2219/n-B4C/MoS<sub>2</sub> hybrid metal matrix composites. *Compos Commun* 2020;19:61–73.
- [35] Kumar S, Sarma VS, Murty B. High temperature wear behavior of Al–4Cu–TiB<sub>2</sub> in situ composites. *Wear* 2010;268(11–12):1266–74.
- [36] Aydin F, Turan ME. The effect of boron nitride on tribological behavior of Mg matrix composite at room and elevated temperatures. *J Tribol* 2020;142(1): 011601.
- [37] Manakari V, et al. Tribological response of magnesium/glass microballoon syntactic foams. In: *Metal-matrix composites: advances in processing, characterization, performance and analysis*. Springer; 2022. p. 311–20.